

Electronic Supplementary Information for Structural Disorder, Anisotropic Microstrain and Cation Vacancies in Thermoelectric Lead Chalcogenides

Sebastian Christensen,¹ Niels Bindzus,¹ Mattia Sist,¹ Masaki Takata² and Bo Brummerstedt Iversen¹

¹Center for Materials Crystallography, Department of Chemistry and iNANO, Aarhus University, Langelandsgade 140, Aarhus C 8000, Denmark

²Japan Synchrotron Radiation Research Institute, I-I-I, Kouto, Sayo-cho, Sayo-gun, Hyogo 679-5198, Japan

Contents

| | | |
|------|--|----|
| I. | Temperature Dependence of Microstrain | 1 |
| II. | Gram-Charlier Modelling of Simulated Data | 2 |
| III. | Pressure Induced Phase Transition | 3 |
| IV. | Anion Mediated <i>s-p</i> Hybridization | 4 |
| V. | Refinement Tables | 6 |
| A. | Le Bail Refinement | 6 |
| 1. | PbS [A] | 6 |
| 2. | PbS [B] | 7 |
| 3. | PbSe | 8 |
| 4. | PbTe | 9 |
| B. | Gram-Charlier Rietveld Refinement | 10 |
| 1. | PbS [A] | 10 |
| 2. | PbS[B] | 11 |
| 3. | PbSe | 12 |
| 4. | PbTe | 13 |
| VI | Structure factor calculation with and without cation defects | 14 |
| | References | 15 |

I. Temperature Dependence of Microstrain

The anisotropic strain parameters for all samples remain approximately constant up to 350 K – 375 K, above which they steadily decrease, Figure S1a,b. The anisotropic character of the strain, however, persists even at the highest temperatures. The observed decrease of strain is model-independently confirmed by extracting the integral breadth

of (400)- and (440)-reflections from Pseudo-Voigt fits to these isolated peaks, Figure S1c. The integral breadths of both reflections clearly decrease above 350 K. It therefore confirms that the total microstrain decreases.

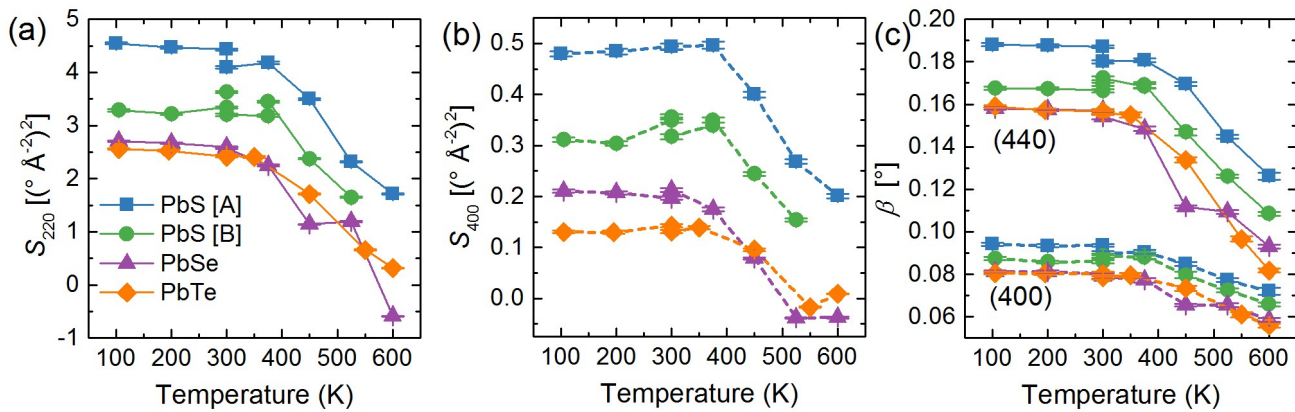


Figure S1 (a,b) Anisotropic strain parameters S_{400} and S_{220} refined by LeBail modelling of PXRD data. (c) Integral breadth of the (400) and (440) peaks obtain by fitting a single Pseudo-Voigt function to these well separated peaks.

II. Gram-Charlier Modelling of Simulated Data

The ability of the Gram-Charlier (GC) expansion to resolve small displacement of Pb is tested by refining the GC-model against simulated PXRD data of PbTe with Pb displaced by $\delta = 0, 0.13 \text{ Å}, 0.26 \text{ Å}$ ($\delta = 0, 0.02, 0.04$ in fractional coordinates). Simulated data were taken from Christensen *et al.*¹ The true probability distribution functions (p.d.f) of the model structure (Figure S2 top) are compared with the p.d.f.s obtained by refining the GC-model against simulated data (Figure S2 bottom). The ordered structure, *i.e.*, $\delta = 0$ is reconstructed without introducing any artefacts. For $\delta = 0.26 \text{ Å}$ the GC-model captures the isolated off-center maxima at, whereas the maxima at $\delta = 0.13 \text{ Å}$ are too poorly resolved to be directly visualized. For a given sample, the lower detection limit depends on the $\sin(\theta)/\lambda$ -resolution, the amount of thermal motion and the magnitude of the off-centering. We apply the Gram-Charlier model to experimental data in section 2.3.1 of the main article.

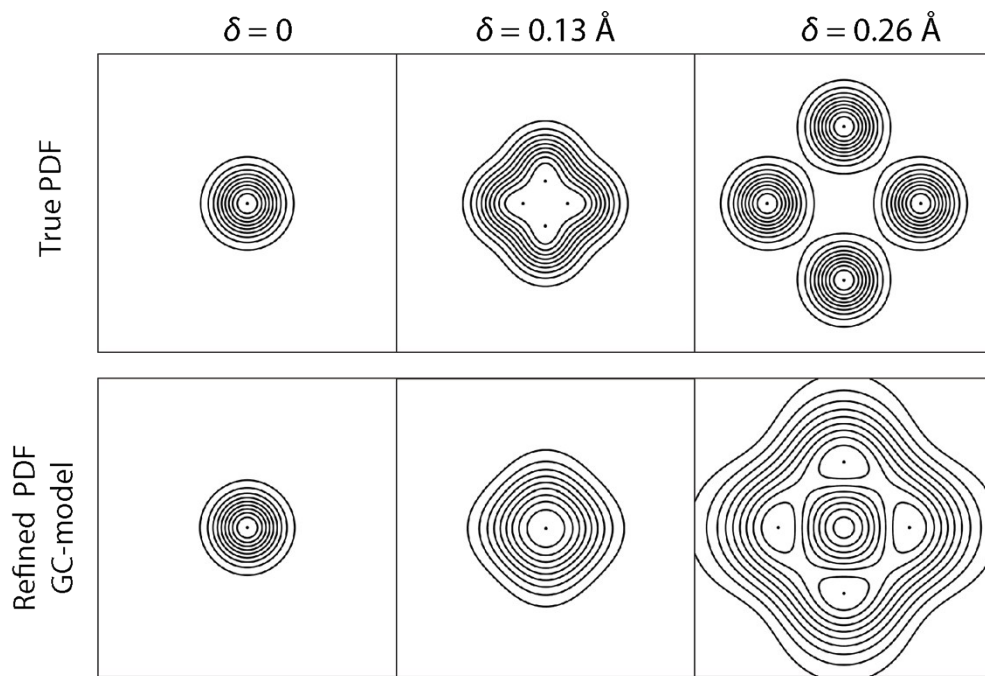


Figure S2 Evaluating the ability of the GC-expansion to detect local disorder. (top) The true p.d.f. of three model structures with Pb sites defined by $(\frac{1}{2}+\delta, \frac{1}{2}, \frac{1}{2})$. (bottom) p.d.f.'s obtained by refining the GC-model against simulated data. The contour plots cover an area of $1 \text{ \AA} \times 1 \text{ \AA}$ in the (100) crystal plane. The contour levels are drawn as $i \times (\rho_{max} - \rho_{min})/10$, $i = 1, 2, \dots, 10$.

III. Pressure Induced Phase Transition

To confirm the phase transition pressure of PbS, PbSe, PbTe, we collected powder X-ray diffraction data on these compounds under high pressure in a diamond anvil cell. The diffractometer was a Supernova (Agilent Technologies) with a Mo-source. A 4:1 methanol-ethanol mixture was used as pressure transmitting medium. The pressure was measured by the Raman line shift of a ruby. The samples were synthesized by same methods as described in section 4.1 of main article but not from same batch entailing that the vacancy concentration – especially of PbS – may be different from the samples studied by synchrotron PXRD.

The cubic to orthorhombic phase transition is initiated at 3.3 GPa (PbS), 5.2 GPa (PbSe) and 6.1 GPa (PbTe), Figure S3. The scattering at $2\theta \approx 21^\circ$ stem from the tungsten gasket. The phase transition was rather sluggish and full conversion was achieved over ~ 1 GPa. Data quality is insufficient for structural refinement or structure solution.

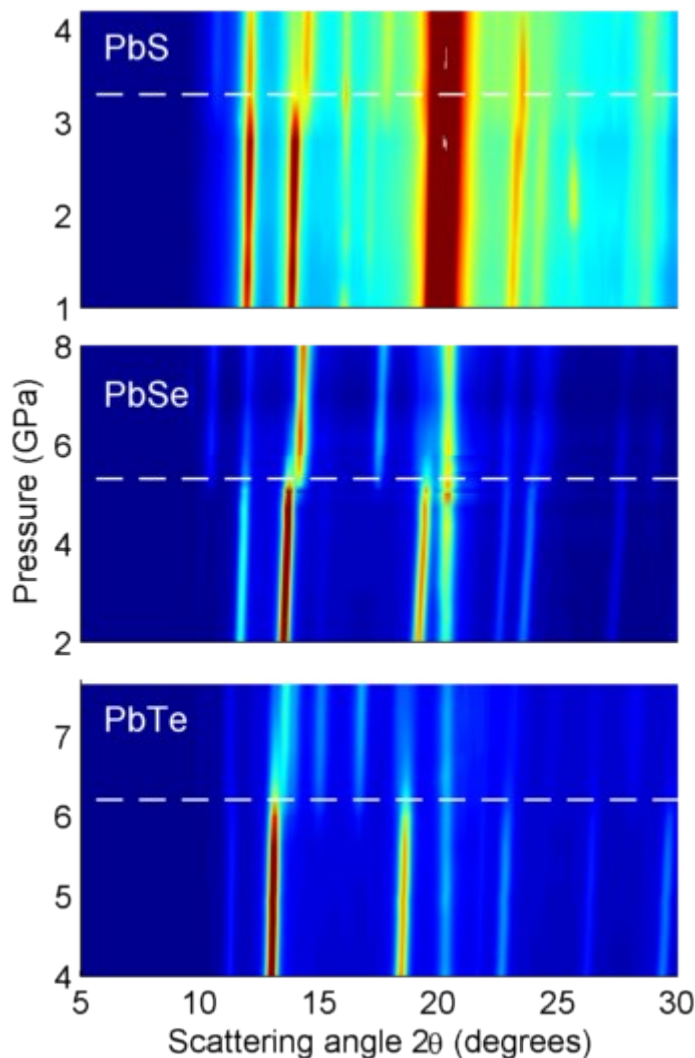


Figure S3 Powder diffraction data for PbS (top), PbSe (middle) and PbTe (bottom) at different pressures.

IV. Anion Mediated *s-p* Hybridization

The driving force for the local distortion and subsequent phase transition may be explained by formation of a sterically active lone pair as described by Walsh and Watson.² A range of Sn(II) and Pb(II) compounds are known to produce asymmetric electron density. The asymmetry is created by hybridization between the *s*- and *p*-orbitals. Walsh and Watson^{2, 3} proposed that the cation *s-p* hybridization is mediated through the anion *p*-orbital. The degree of interaction can be qualitatively explained by using an orbital interaction diagram, Figure S4 adapted from ref. Walsh and Watson². Orbital energies calculated by scalar-relativistic local-density approximation (ScRLDA) are included in the figure.⁴

The Sn(5s)/Pb(6s) interact with anion *p* states to form the filled antibonding states SP*. These states can couple to Sn(5p)/Pb(6p), and form SSP/SSP*, which is an *s-p*-hybridization mediated by the anion.²

Ascending through the chalcogenide group, the Pb(6s) and Te(5p)/Se(4p)/S(3p)/O(2p)-states moves closer, thus increasing the coupling resulting in larger *s-p* hybridization. Only for PbO is the interaction sufficiently strong to distort the long range structure at ambient pressure. For PbTe, PbSe, and PbS this covalent interaction is insufficient to distort the long range structure. Instead it is revealed by local distortions of the structure which induces anisotropic strain as observed experimentally.

The Pb(6s)-states are – compared to Sn(5s) – further away from the chalcogenide *p*-states. Thus, it is expected that *s-p* hybridization will be weaker for PbX compared to SnX. This agrees well with the observation that all lead chalcogenides (except PbO) have the rock-salt structure while for tin chalcogenides only SnTe crystallizes in the rock-salt structure at ambient conditions.

Beyond the simple picture illustrated by Figure S4 various effect must influence the phase transition since the lead chalcogenides adapt different structures at high pressure: PbS(B33, *Cmcm*),⁵ PbSe (B33, *Cmcm*),⁵ PbTe(*Pnma*).⁶

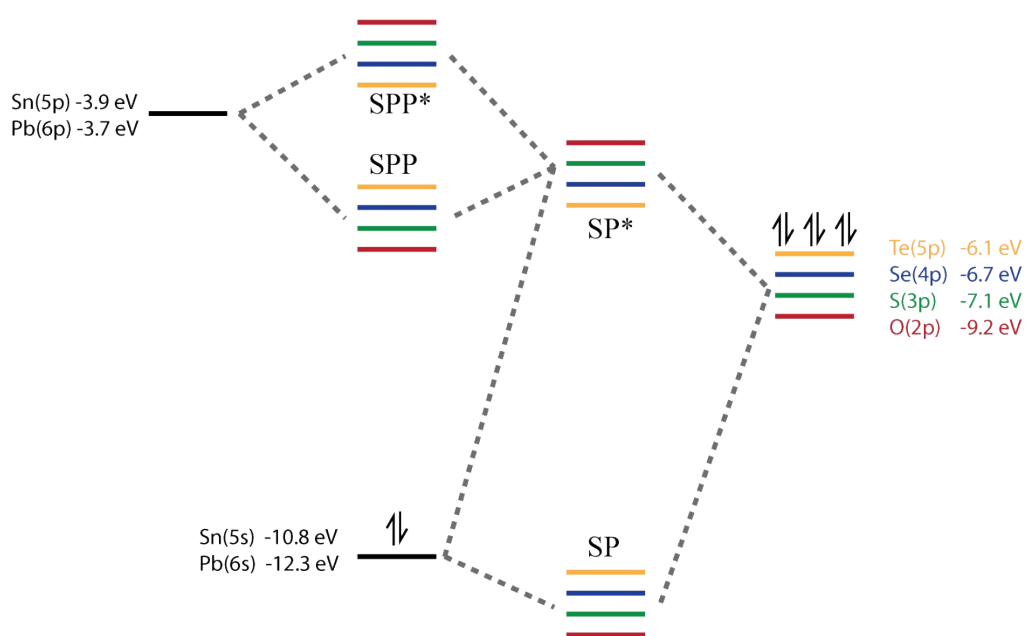


Figure S4 Schematic illustration of how coupling between cation *s* and *p* states is mediated by anion *p*-states. Orbital energies from Tanaka *et al.*⁴. The positions of energy levels are not drawn to scale.

V. Refinement Tables

All refined parameters are reported for LeBail and Rietveld refinements of all datasets. In both case the peak profile includes anisotropic strain broadening. Note that the definition of strain coefficients in JANA2006 differ from the original definition by Stephens⁷ as discussed by Leineweber and Mittemeijer.⁸ The coefficients are converted as: $S_{400}^{Stephens} = S_{400}^{JANA}$, $S_{220}^{Stephens} = 6S_{220}^{JANA}$. In the main article and Figure S1 we report strain coefficients as they are defined by Stephens. The Rietveld model includes vacancies on the Pb-site and Gram-Charlier expansion of thermal parameters of Pb. Profile parameters marked with “(−)” are kept fixed to the value of the CeO₂-standard sample.

A. Le Bail Refinement

| 1. PbS [A] | | | | | | | | |
|--------------------------------------|-------------|-------------|-------------|-------------|-------------|-------------|-------------|-------------|
| | 100 K - LT | 200 K - LT | 300 K - LT | 300 K - HT | 375 K - HT | 450 K - HT | 525 K - HT | 600 K - HT |
| a (Å) | 5.91170(3) | 5.92296(3) | 5.93465(3) | 5.93424(4) | 5.94290(4) | 5.95106(4) | 5.95941(4) | 5.96838(4) |
| Zeros shift | 0.467(10) | -0.108(10) | 0.04(1) | -0.88(1) | -0.73(1) | -1.59(1) | -1.35(1) | -0.87(1) |
| GU | 1.695108(−) | 1.695108(−) | 1.695108(−) | 1.695108(−) | 1.695108(−) | 1.695108(−) | 1.695108(−) | 1.695108(−) |
| GW | 1.87(2) | 1.76(2) | 1.70(2) | 1.43(2) | 1.43(2) | 1.44(2) | 1.47(2) | 1.46(2) |
| LX | 0.967686(−) | 0.967686(−) | 0.967686(−) | 0.967686(−) | 0.967686(−) | 0.967686(−) | 0.967686(−) | 0.967686(−) |
| LY | 1.173841(−) | 1.173841(−) | 1.173841(−) | 1.173841(−) | 1.173841(−) | 1.173841(−) | 1.173841(−) | 1.173841(−) |
| asym | 0.00102(5) | 0.00105(5) | 0.00105(5) | 0.00051(6) | 0.00048(6) | 0.00063(6) | 0.00088(6) | 0.00135(7) |
| ζ | 0.711(2) | 0.707(2) | 0.707(2) | 0.722(3) | 0.737(3) | 0.734(3) | 0.738(4) | 0.740(5) |
| $S_{400}^{JANA} (\text{° Å}^{-2})^2$ | 0.480(5) | 0.484(5) | 0.494(5) | 0.494(6) | 0.496(7) | 0.400(6) | 0.269(5) | 0.201(4) |
| $S_{220}^{JANA} (\text{° Å}^{-2})^2$ | 0.758(3) | 0.745(3) | 0.738(3) | 0.683(4) | 0.697(4) | 0.583(4) | 0.386(3) | 0.286(3) |
| R_p (%) | 1.38 | 1.33 | 1.28 | 1.55 | 1.57 | 1.49 | 1.41 | 1.55 |
| R_{wp} (%) | 2.2 | 2.16 | 2.12 | 2.23 | 2.27 | 2.18 | 2.12 | 2.32 |

| 2. PbS [B] | | 105 K – LT Glass | 200 K – LT Glass | 300 K – LT Glass | 300 K – HT Glass | 300 K – HT Quartz | 375 K – HT Glass | 375 K – HT Quartz | 450 K – HT Quartz | 525 K – HT Quartz | 600 K – HT Quartz* |
|-------------------------------------|-------------|---------------------|---------------------|---------------------|---------------------|----------------------|---------------------|----------------------|----------------------|----------------------|-----------------------|
| a (Å) | 5.91218(3) | 5.92281(3) | 5.93442(4) | 5.93429(4) | 5.93535(3) | 5.94364(4) | 5.94494(4) | 5.95462(3) | 5.96501(3) | 5.97646(3) | |
| Zeros shift | 1.55(1) | 1.45(1) | 2.30(1) | 1.55(1) | 1.69(1) | 1.94(1) | 1.66(1) | 1.69(1) | 1.800(10) | 1.552(9) | |
| GU | 4.304461(-) | 4.304461(-) | 4.304461(-) | 4.304461(-) | 4.304461(-) | 4.304461(-) | 4.304461(-) | 4.304461(-) | 4.304461(-) | 4.304461(-) | 4.304461(-) |
| GW | 1.88(2) | 1.74(2) | 1.73(2) | 1.73(2) | 1.71(2) | 1.78(2) | 1.74(2) | 1.70(2) | 1.75(1) | 2.23(1) | |
| LX | 0.951925(-) | 0.951925(-) | 0.951925(-) | 0.951925(-) | 0.951925(-) | 0.951925(-) | 0.951925(-) | 0.951925(-) | 0.951925(-) | 0.951925(-) | 0.951925(-) |
| LY | 1.396012(-) | 1.396012(-) | 1.396012(-) | 1.396012(-) | 1.396012(-) | 1.396012(-) | 1.396012(-) | 1.396012(-) | 1.396012(-) | 1.396012(-) | 1.396012(-) |
| asym | 0.00094(6) | 0.00093(6) | 0.00102(6) | 0.00110(6) | 0.00106(5) | 0.00113(6) | 0.00112(5) | 0.00158(5) | 0.00192(5) | 0.00094(5) | |
| ζ | 0.663(3) | 0.654(3) | 0.659(3) | 0.661(3) | 0.687(3) | 0.656(3) | 0.682(3) | 0.660(3) | 0.676(4) | 0.6634(-) | |
| $S_{400}^{ANA} (\text{° Å}^{-2})^2$ | 0.312(5) | 0.304(5) | 0.318(5) | 0.350(5) | 0.356(5) | 0.340(5) | 0.350(5) | 0.244(4) | 0.154(3) | 0.311(1) | |
| $S_{220}^{ANA} (\text{° Å}^{-2})^2$ | 0.548(3) | 0.537(3) | 0.534(3) | 0.557(3) | 0.605(3) | 0.531(3) | 0.575(3) | 0.396(2) | 0.275(2) | 0.548(1) | |
| R_p (%) | 1.84 | 1.77 | 1.67 | 1.51 | 1.32 | 1.46 | 1.25 | 1.19 | 1.18 | 1.94 | |
| R_{wp} (%) | 3.04 | 3.01 | 2.87 | 2.55 | 2.22 | 2.5 | 2.13 | 2.03 | 1.99 | 3.72 | |

*600 K this sample of PbS is partly oxidized to orthorhombic PbSO₄. The secondary phase makes refinement of anisotropic strain unreliable.

3. PbSe

| | 105 K - LT | 200 K - LT | 300 K - LT | 300 K - HT | 375 K - HT | 450 K - HT | 525 K - HT | 600 K - HT |
|-------------------------------------|-------------------|-------------------|-------------------|-------------------|-------------------|-------------------|-------------------|-------------------|
| <i>a</i> (Å) | 6.10257(2) | 6.11422(3) | 6.12642(3) | 6.12638(3) | 6.13599(4) | 6.14567(3) | 6.15581(4) | 6.16732(3) |
| Zeros shift | 0.176(9) | 1.043(9) | 0.63(1) | 0.81(1) | 0.26(1) | 0.788(10) | 1.44(1) | 1.354(10) |
| <i>GU</i> | 4.304461(-) | 4.304461(-) | 4.304461(-) | 4.304461(-) | 4.304461(-) | 4.304461(-) | 4.304461(-) | 4.304461(-) |
| <i>GW</i> | 2.09(2) | 2.05(2) | 2.03(2) | 1.76(2) | 1.86(2) | 1.78(1) | 2.05(2) | 1.67(1) |
| <i>LX</i> | 0.951925(-) | 0.951925(-) | 0.951925(-) | 0.951925(-) | 0.951925(-) | 0.951925(-) | 0.951925(-) | 0.951925(-) |
| <i>LY</i> | 1.396012(-) | 1.396012(-) | 1.396012(-) | 1.396012(-) | 1.396012(-) | 1.396012(-) | 1.396012(-) | 1.396012(-) |
| asym | 0.00131(5) | 0.00110(5) | 0.00139(6) | 0.00126(6) | 0.00131(6) | 0.00213(6) | 0.00215(6) | 0.00246(6) |
| ζ | 0.662(2) | 0.659(3) | 0.655(3) | 0.662(3) | 0.653(4) | 0.668(4) | 0.691(7) | 0.668(7) |
| $S_{400}^{ANA} (\text{° Å}^{-2})^2$ | 0.210(3) | 0.207(3) | 0.197(3) | 0.213(3) | 0.175(3) | 0.079(2) | -0.038(2) | -0.037(1) |
| $S_{220}^{ANA} (\text{° Å}^{-2})^2$ | 0.450(2) | 0.445(2) | 0.433(2) | 0.428(2) | 0.375(2) | 0.190(1) | 0.199(2) | -0.098(1) |
| <i>R_p</i> (%) | 1.29 | 1.21 | 1.27 | 1.19 | 1.18 | 1.16 | 1.29 | 1.11 |
| <i>R_{wp}</i> (%) | 2.14 | 2.11 | 2.23 | 1.99 | 2.01 | 1.99 | 2.23 | 2.00 |

4. PbTe

| | 105 K - LT | 195 K - LT | 300 K - LT | 300 K - HT | 350 K - HT | 450 K - HT | 550 K - HT | 600 K - HT |
|-------------------------------------|-------------------|-------------------|-------------------|-------------------|-------------------|-------------------|-------------------|-------------------|
| <i>a</i> (Å) | 6.43549(3) | 6.44692(3) | 6.46040(4) | 6.46054(4) | 6.46669(4) | 6.47865(4) | 6.49051(4) | 6.49667(3) |
| Zeros shift | 1.25(1) | 0.88(1) | 0.48(1) | 1.24(1) | 1.35(1) | 1.65(1) | 1.59(1) | 0.98(1) |
| <i>GU</i> | 1.153684(-) | 1.153684(-) | 1.153684(-) | 1.153684(-) | 1.153684(-) | 1.153684(-) | 1.153684(-) | 1.153684(-) |
| <i>GW</i> | 2.11(2) | 2.08(2) | 2.03(2) | 1.77(2) | 1.84(2) | 1.73(2) | 1.70(1) | 1.51(1) |
| <i>LX</i> | 1.219802(-) | 1.219802(-) | 1.219802(-) | 1.219802(-) | 1.219802(-) | 1.219802(-) | 1.219802(-) | 1.219802(-) |
| <i>LY</i> | 1.883540(-) | 1.883540(-) | 1.883540(-) | 1.883540(-) | 1.883540(-) | 1.883540(-) | 1.883540(-) | 1.883540(-) |
| asym | 0.00194(6) | 0.00178(6) | 0.00160(6) | 0.00127(6) | 0.00121(6) | 0.00129(6) | 0.00207(7) | 0.00253(6) |
| ζ | 0.687(3) | 0.696(3) | 0.688(3) | 0.703(4) | 0.711(4) | 0.763(5) | 0.79(1) | 0.74(1) |
| $S_{400}^{ANA} (\text{° Å}^{-2})^2$ | 0.131(3) | 0.130(3) | 0.131(3) | 0.142(3) | 0.139(3) | 0.095(2) | -0.017(1) | 0.0092(7) |
| $S_{220}^{ANA} (\text{° Å}^{-2})^2$ | 0.426(2) | 0.422(2) | 0.406(2) | 0.402(2) | 0.401(2) | 0.285(2) | 0.110(2) | 0.054(1) |
| <i>R_p</i> (%) | 2.05 | 1.69 | 1.57 | 1.69 | 1.64 | 1.77 | 1.63 | 1.57 |
| <i>R_{wp}</i> (%) | 3.24 | 2.84 | 2.65 | 2.88 | 2.80 | 2.72 | 2.89 | 2.80 |

B. Gram-Charlier Rietveld Refinement**1. PbS [A]**

| Parameter | 100 K - LT | 200 K - LT | 300 K - LT | 300 K - HT | 375 K - HT | 450 K - HT | 525 K - HT | 600 K - HT |
|--|-------------------|-------------------|-------------------|-------------------|-------------------|-------------------|-------------------|-------------------|
| <i>a</i> (Å) | 5.91168(2) | 5.92293(3) | 5.93462(3) | 5.93421(4) | 5.94287(4) | 5.95102(4) | 5.95937(4) | 5.96832(4) |
| Occ.(Pb) | 0.978(2) | 0.986(2) | 0.973(3) | 0.965(3) | 0.969(3) | 0.974(3) | 0.952(3) | 0.954(4) |
| <i>U</i>_{iso}(Pb)[Å²] | 0.00505(5) | 0.00964(7) | 0.01427(9) | 0.0138(1) | 0.0169(1) | 0.0205(1) | 0.0248(2) | 0.0284(2) |
| <i>D</i>₁₁₂₂ | -0.00031(3) | -0.00041(6) | -0.00068(9) | -0.0013(1) | -0.0018(2) | -0.0019(2) | -0.0016(2) | -0.0024(3) |
| <i>U</i>_{iso}(Te)[Å²] | 0.0065(2) | 0.0099(2) | 0.0153(3) | 0.0147(4) | 0.0177(4) | 0.0211(5) | 0.0264(5) | 0.0308(7) |
| zero shift | 0.489(9) | -0.087(9) | 0.065(10) | -0.86(1) | -0.71(1) | -1.57(1) | -1.32(1) | -0.83(1) |
| Scale | 0.2641(6) | 0.2620(7) | 0.2679(7) | 0.1078(4) | 0.1067(4) | 0.1057(4) | 0.1083(4) | 0.1064(4) |
| <i>GW</i> | 2.72(2) | 2.59(2) | 2.51(2) | 2.20(2) | 2.20(2) | 2.15(2) | 2.05(2) | 1.95(2) |
| <i>LY</i> | 26.7(1) | 26.9(1) | 27.3(1) | 27.3(2) | 27.6(2) | 25.7(2) | 23.148430(-) | 21.7(1) |
| asym | 0.00112(5) | 0.00116(5) | 0.00114(5) | 0.00058(6) | 0.00056(6) | 0.00074(6) | 0.00103(6) | 0.00154(7) |
| ζ | 0.587(6) | 0.596(6) | 0.603(6) | 0.630(9) | 0.69(1) | 0.71(1) | 0.8(5) | 0.799728(-) |
| <i>S</i>₄₀₀^{IANA}(° Å⁻²)² | -0.080(4) | -0.080(4) | -0.077(5) | -0.071(5) | -0.069(6) | -0.059(5) | -0.062(4) | -0.071(4) |
| <i>S</i>₂₂₀^{IANA}(° Å⁻²)² | 0.265(3) | 0.261(3) | 0.254(3) | 0.220(3) | 0.215(4) | 0.177(4) | 0.101(5) | 0.076(2) |
| <i>R</i>_F (%) | 0.75 | 0.84 | 0.83 | 1.5 | 1.67 | 1.6 | 1.34 | 1.39 |
| <i>R</i>_{wF} (%) | 0.8 | 0.72 | 0.82 | 0.95 | 0.92 | 1.04 | 0.97 | 1.01 |
| <i>R</i>_p (%) | 1.30 | 1.23 | 1.17 | 1.49 | 1.47 | 1.40 | 1.37 | 1.49 |
| <i>R</i>_{wp} (%) | 2.09 | 2.01 | 1.95 | 2.16 | 2.16 | 2.08 | 2.09 | 2.27 |

2. PbS[B]

| Parameter | 105 K – LT Glass | 105 K – LT Glass Full occupancy† | 200 K – LT Glass | 300 K – LT Glass | 300 K – HT Glass | 300 K – HT Quartz | 375 K – HT Glass | 375 K – HT Quartz | 450 K – HT Quartz | 525 K – HT Quartz | 600 K – HT Quartz* |
|---|------------------|-------------------------------------|------------------|------------------|------------------|-------------------|------------------|-------------------|-------------------|-------------------|--------------------|
| <i>a</i> (Å) | 5.91218(3) | 5.91217(3) | 5.92281(3) | 5.93442(3) | 5.93428(3) | 5.93532(3) | 5.94364(3) | 5.94491(3) | 5.95458(3) | 5.96495(3) | |
| Occ.(Pb) | 0.958(3) | 1.000(-) | 0.953(3) | 0.949(3) | 0.949(3) | 0.927(3) | 0.937(3) | 0.929(3) | 0.927(3) | 0.926(3) | 0.915(3) |
| $U_{\text{iso}}(\text{Pb})[\text{\AA}^2]$ | 0.00412(6) | 0.00412(3) | 0.00805(8) | 0.0127(1) | 0.01211(10) | 0.01181(9) | 0.0159(1) | 0.0157(1) | 0.0195(1) | 0.0243(1) | 0.0295(2) |
| D_{1122} | -0.00036(4) | -0.00036(4) | -0.00070(6) | -0.0010(1) | -0.00143(10) | -0.00189(9) | -0.0017(1) | -0.0024(1) | -0.0030(2) | -0.0033(2) | -0.0039(4) |
| $U_{\text{iso}}(\text{S})[\text{\AA}^2]$ | 0.0068(2) | 0.0048(2) | 0.0108(3) | 0.0158(4) | 0.0145(3) | 0.0166(3) | 0.0203(4) | 0.0209(4) | 0.0251(4) | 0.0296(4) | 0.0365(6) |
| zero shift | 1.55(1) | 1.55(1) | 1.46(1) | 2.30(1) | 1.55(1) | 1.710(10) | 1.95(1) | 1.679(10) | 1.723(9) | 1.834(9) | 2.263(10) |
| Scale | 0.2992(9) | 0.2866(2) | 0.3021(10) | 0.307(1) | 0.2847(9) | 0.2692(8) | 0.2913(9) | 0.2683(8) | 0.2658(8) | 0.2670(8) | 0.2713(9) |
| GW | 2.77(2) | 2.78(2) | 2.60(2) | 2.55(2) | 2.57(2) | 2.51(2) | 2.62(2) | 2.53(2) | 2.38(1) | 2.37(1) | 2.23(1) |
| LY | 21.6(1) | 21.5(1) | 21.6(1) | 22.3(1) | 23.1(1) | 23.8(1) | 22.9(1) | 23.7(1) | 21.3(1) | 15.3(2) | 16.7(1) |
| asym | 0.00094(6) | 0.00093(6) | 0.00094(6) | 0.00104(6) | 0.00113(5) | 0.00116(5) | 0.00116(5) | 0.00121(5) | 0.00173(5) | 0.00211(5) | 0.00263(5) |
| ζ | 0.589(6) | 0.597(6) | 0.592(7) | 0.604(7) | 0.588(7) | 0.620(7) | 0.596(7) | 0.621(7) | 0.601(8) | 0.79(1) | 0.78(-) |
| $S_{400}^{IANA}([\text{\AA}^{-2}]^2)$ | -0.026028(-) | -0.026028(-) | -0.019(5) | -0.025(5) | -0.035(5) | -0.041(4) | -0.023(5) | -0.040(5) | -0.045(3) | -0.015(2) | -0.022(1) |
| $S_{220}^{IANA}([\text{\AA}^{-2}]^2)$ | 0.216(3) | 0.220(3) | 0.213(3) | 0.206(3) | 0.213(3) | 0.225(3) | 0.198(3) | 0.212(3) | 0.148(2) | 0.132(5) | 0.048(1) |
| R_F (%) | 0.71 | 0.68 | 0.78 | 0.96 | 1.50 | 1.54 | 1.36 | 1.25 | 1.52 | 1.24 | 1.42 |
| R_{wF} (%) | 0.82 | 0.70 | 0.92 | 0.93 | 1.55 | 1.38 | 1.33 | 1.16 | 1.34 | 1.21 | 1.66 |
| R_p (%) | 1.72 | 1.71 | 1.63 | 1.53 | 1.55 | 1.24 | 1.34 | 1.18 | 1.13 | 1.06 | 1.30 |
| R_{wp} (%) | 2.82 | 2.86 | 2.69 | 2.57 | 2.68 | 2.01 | 2.21 | 1.94 | 1.85 | 1.8 | 2.41 |

†By forcing full occupancy of Pb, $U_{\text{iso}}(\text{S})$ decreases and the scale decreases. This combination effectively corresponds to decreasing the relative scattering power of Pb. R_F and R_{wF} are slightly reduced compared to the model with lead vacancies; however the unphysically low $U_{\text{iso}}(\text{S})$ for the full occupancy model as discussed in section 2.2 of main article.

* 600 K this sample of PbS is partly oxidized to orthorhombic PbSO₄. Refinement shows 5.5(2) % PbSO₄.

3. PbSe

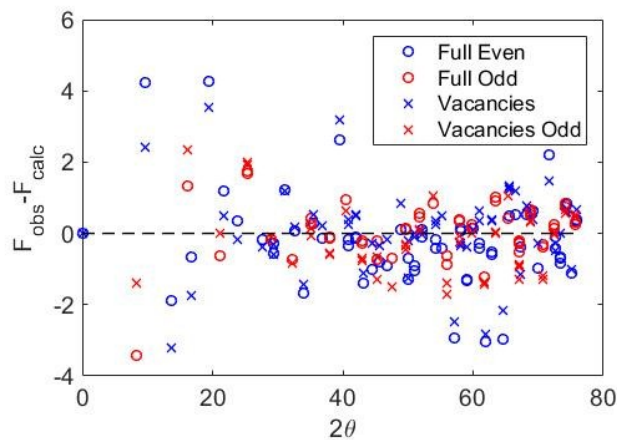
| Parameter | 105 K - LT | 200 K - LT | 300 K - LT | 300 K - HT | 375 K - HT | 450 K - HT | 525 K - HT | 600 K - HT |
|--|-------------------|-------------------|-------------------|-------------------|-------------------|-------------------|-------------------|-------------------|
| <i>a</i> (Å) | 6.10255(2) | 6.11420(2) | 6.12640(3) | 6.12636(3) | 6.13597(3) | 6.14564(3) | 6.15583(3) | 6.16730(3) |
| Occ.(Pb) | 0.992(1) | 0.993(1) | 0.993(1) | 0.982(1) | 0.987(1) | 0.987(1) | 0.985(2) | 0.979(2) |
| <i>U</i>_{iso}(Pb)[Å²] | 0.00559(6) | 0.00993(8) | 0.0151(1) | 0.0152(1) | 0.0201(2) | 0.0252(2) | 0.0293(2) | 0.0360(2) |
| <i>D</i>₁₁₂₂ | -0.00033(4) | -0.00082(6) | -0.0011(1) | -0.0010(1) | -0.0012(2) | -0.0011(2) | -0.0024(3) | -0.0023(3) |
| <i>U</i>_{iso}(Se)[Å²] | 0.00477(9) | 0.0081(1) | 0.0121(2) | 0.0129(2) | 0.0166(2) | 0.0208(2) | 0.0249(2) | 0.0310(3) |
| zero shift | 0.192(8) | 1.061(8) | 0.657(9) | 0.832(9) | 0.27(1) | 0.807(9) | 1.441(10) | 1.369(10) |
| Scale | 0.2816(3) | 0.2836(3) | 0.2849(4) | 0.2160(3) | 0.2155(3) | 0.2154(3) | 0.2158(3) | 0.2193(4) |
| <i>GW</i> | 2.63(2) | 2.63(2) | 2.63(2) | 2.36(2) | 2.39(2) | 2.16(1) | 2.20(2) | 1.91(1) |
| <i>LY</i> | 18.7(2) | 20.0(2) | 20.2(2) | 20.3(2) | 19.1(3) | 14.1(2) | 13.6(2) | 10.3(2) |
| asym | 0.00140(5) | 0.00122(5) | 0.00154(5) | 0.00135(5) | 0.00139(6) | 0.00225(5) | 0.00218(6) | 0.00256(6) |
| ζ | 0.516(5) | 0.531(6) | 0.548(6) | 0.541(7) | 0.558(8) | 0.61(1) | 0.60(1) | 0.65(2) |
| <i>S</i>₄₀₀^{JANA}(° Å⁻²)² | -0.017(3) | -0.020(4) | -0.016(5) | -0.023(5) | -0.022(5) | -0.016(3) | 0.000000(-) | 0.000000(-) |
| <i>S</i>₂₂₀^{JANA}(° Å⁻²)² | 0.185(2) | 0.177(2) | 0.172(2) | 0.169(2) | 0.154(2) | 0.076(2) | 0.064(2) | 0.035(1) |
| <i>R</i>_F (%) | 0.89 | 1.07 | 0.86 | 1.19 | 0.6 | 0.75 | 0.98 | 1.13 |
| <i>R</i>_{wF} (%) | 0.89 | 0.85 | 0.83 | 0.95 | 0.7 | 0.9 | 0.87 | 1.16 |
| <i>R</i>_p (%) | 1.25 | 1.12 | 1.17 | 1.09 | 1.13 | 1.07 | 1.07 | 1.05 |
| <i>R</i>_{wp} (%) | 2.03 | 1.92 | 2.00 | 1.84 | 1.86 | 1.84 | 1.87 | 1.91 |

4. PbTe

| Parameter | 105 K - LT | 195 K - LT | 300 K - LT | 300 K - HT | 350 K - HT | 450 K - HT | 550 K - HT | 600 K - HT |
|--|-------------------|-------------------|-------------------|-------------------|-------------------|-------------------|-------------------|-------------------|
| <i>a</i> (Å) | 6.43550(3) | 6.44692(3) | 6.46040(3) | 6.46053(4) | 6.46668(4) | 6.47863(4) | 6.49053(4) | 6.49666(3) |
| Occ.(Pb) | 0.993(1) | 0.992(1) | 0.992(1) | 0.993(1) | 0.993(1) | 0.993(1) | 0.992(2) | 0.991(2) |
| <i>U</i>_{iso}(Pb)[Å²] | 0.00806(10) | 0.0136(1) | 0.0202(1) | 0.0199(2) | 0.0234(2) | 0.0307(2) | 0.0390(3) | 0.0430(3) |
| <i>D</i>₁₁₂₂ | -0.00030(6) | -0.00062(8) | -0.0012(1) | -0.0013(1) | -0.0013(2) | -0.0017(3) | -0.0011(4) | -0.0015(4) |
| <i>U</i>_{iso}(Te)[Å²] | 0.0055(1) | 0.0093(1) | 0.0141(2) | 0.0136(2) | 0.0159(2) | 0.0210(2) | 0.0272(3) | 0.0301(3) |
| zero shift | 1.25(1) | 0.882(10) | 0.49(1) | 1.26(1) | 1.37(1) | 1.67(1) | 1.59(1) | 0.995(10) |
| Scale | 0.2323(3) | 0.2352(2) | 0.2403(3) | 0.2253(3) | 0.2256(3) | 0.2276(3) | 0.2294(3) | 0.2311(3) |
| <i>GW</i> | 2.60(2) | 2.56(2) | 2.51(2) | 2.22(2) | 2.29(2) | 2.07(2) | 1.76(1) | 1.65(1) |
| <i>LY</i> | 19.0(3) | 20.0(3) | 20.1(3) | 21.1(3) | 21.4(3) | 18.1(3) | 11.4(2) | 9.2(2) |
| asym | 0.00197(6) | 0.00181(5) | 0.00165(5) | 0.00142(6) | 0.00135(6) | 0.00145(6) | 0.00211(6) | 0.00267(6) |
| ζ | 0.599(6) | 0.623(6) | 0.623(7) | 0.627(8) | 0.650(8) | 0.73(1) | 0.728081(-) | 0.728081(-) |
| <i>S</i>₄₀₀^{IANA}(° Å⁻²)² | -0.039(4) | -0.036(4) | -0.028(4) | -0.028(5) | -0.030(5) | -0.023(4) | 0.000000(-) | 0.000000(-) |
| <i>S</i>₂₂₀^{IANA}(° Å⁻²)² | 0.195(3) | 0.184(2) | 0.175(3) | 0.159(3) | 0.156(3) | 0.100(3) | 0.035(1) | 0.0182(7) |
| <i>R</i>_F (%) | 0.91 | 1.02 | 1.14 | 1.19 | 1.03 | 1.04 | 0.6 | 0.71 |
| <i>R</i>_{wF} (%) | 1.14 | 1.09 | 1.05 | 1.38 | 1.13 | 1.24 | 1.00 | 1.43 |
| <i>R</i>_p (%) | 2.02 | 1.77 | 1.47 | 1.55 | 1.5 | 1.42 | 1.44 | 1.44 |
| <i>R</i>_{wp} (%) | 3.07 | 2.74 | 2.49 | 2.64 | 2.55 | 2.48 | 2.62 | 2.62 |

VI. Structure factor calculation

Structure factor analysis can sometimes be used to deduce subtle structural details, and it was suggested to us that Pb vacancies can be observed by comparing odd and even reflections. We plotted the difference between observed and calculated structure factors ($F_{obs} - F_{calc}$) for Rietveld models with and without Pb vacancies (PbS [B], 105 K). Overall the vacancy model reduces the difference ($|F_{obs}| - |F_{calc}|$). However there is not a systematic distribution of odd and even reflections.



To understand why vacancies in the structure did not produce a systematic difference to the fully occupied model, we evaluated the structure factors. For the fully occupied structure the form factor is:

$$\begin{array}{ll} \text{All even} & |F_0| = 4(f_{Pb} + f_S) \\ \text{All odd} & |F_0| = 4(f_{Pb} - f_S) \end{array}$$

where $f_{Pb} > f_S$. If the structure contains Pb-vacancies the structure factor is:

$$\begin{array}{ll} \text{All even} & |F_{vac.}| = 4(xf_{Pb} + f_S) \\ \text{All odd} & |F_{vac.}| = 4(xf_{Pb} - f_S) \end{array}$$

where $0 < x < 1$. In the case where the actual structure (F_{obs}) contains vacancies but is refined with the fully occupied structure, then the difference between observed and calculated structure factors is:

$$\begin{array}{ll} \text{All even} & |F_{obs}| - |F_{calc}| = |F_{vac.}| - |F_0| = 4(x-1)f_{Pb} \\ \text{All odd} & |F_{obs}| - |F_{calc}| = |F_{vac.}| - |F_0| = 4(x-1)f_{Pb} \end{array}$$

Therefore the effect of vacancies is not revealed by simply comparing the odd and even reflections. S-vacancies would be more easily observed since they could cause $F_{obs} - F_{calc} < 0$ for even and $F_{obs} - F_{calc} > 0$ for odd reflections. The matter is further complicated by the aspherical distribution of Pb.

References

1. S. Christensen, N. Bindzus, M. Christensen and B. B. Iversen, *Acta Cryst. A*, 2015, **71**, 9-19.
2. A. Walsh and G. W. Watson, *J. Phys. Chem. B*, 2005, **109**, 18868-18875.
3. A. Walsh and G. W. Watson, *J. Solid State Chem.*, 2005, **178**, 1422-1428.
4. H. Tanaka, Y. Kuroiwa and M. Takata, *Phys. Rev. B*, 2006, **74**, 172105.
5. K. Knorr, L. Ehm, M. Hytha, B. Winkler and W. Depmeier, *Eur Phys J B*, 2003, **31**, 297-303.
6. G. Rousse, S. Klotz, A. M. Saitta, J. Rodriguez-Carvajal, M. I. McMahon, B. Couzinet and M. Mezouar, *Phys. Rev. B*, 2005, **71**, 224116.
7. P. W. Stephens, *J. Appl. Crystallogr.*, 1999, **32**, 281-289.
8. A. Leineweber and E. J. Mittemeijer, *J. Appl. Crystallogr.*, 2004, **37**, 123-135.